Applied Catalysis B: Environmental 170-171 (2015) 66–73

Contents lists available at ScienceDirect

Applied Catalysis B: Environmental

journal homepage: www.elsevier.com/locate/apcatb

A facile approach to further improve the substitution of nitrogen into reduced TiO_{2-x} with an enhanced photocatalytic activity

Yi Zhou, Yunchang Liu, Pengwei Liu, Weiyi Zhang, Mingyang Xing*, Jinlong Zhang*

Key Lab for Advanced Materials and Institute of Fine Chemicals, East China University of Science and Technology, Shanghai 200237, China

ARTICLE INFO

Article history:
Received 2 December 2014
Received in revised form 21 January 2015
Accepted 26 January 2015
Available online 28 January 2015

Keywords:
Ti^{3+} doped
TiO_2
Nitrogen doped
Photocatalytic activity

ABSTRACT

A series of nitrogen/Ti^{3+} co-doped titanium dioxides (N–TiO_{2-x}) were successfully synthesized through a calcination–vacuum activation method by using low-cost ammonium hydroxide as the nitrogen source. Interestingly, the nitrogen could be further doped into TiO_2 lattice via the substitution of oxygen vacancies after the vacuum activation treatment. The as-prepared catalysts exhibited high visible light activity by improved substitution of nitrogen concentration with no affecting the UV-light photocatalytic activities. The samples were characterized by the XRD, UV–vis DRS, ESR, XPS and TEM analyzes. When the temperature of vacuum activation was 300 °C, N–TiO_{2-x} catalyst showed the highest photocatalytic activity for the degradation of methyl orange (MO) under the visible light irradiation. The increase in the visible-light photocatalytic activity was attributed to the synergistic effect between Ti^{3+} and nitrogen doping, which contributed to the increase of absorption in the visible light region. It can be claimed that N–TiO_{2-x} (300 °C-3 h) contained the highest concentration of Ti^{3+}.

1. Introduction

Titanium dioxide has been widely used as a remarkable photocatalyst owing to its excellent performance in environmental issue and energy problems, for instance, the degradation of organic pollutant [1–7], purification of noxious gas [8–11], capability of solar energy storage [12–15]. Additionally, it is also one of the most attractive materials due to its low cost, non-toxicity, well stability in chemical and physical [16,17]. The wide band gap of titania (3.0–3.2 eV) limits its photocatalytic application in the UV region, however, there is merely approximately 4% of ultraviolet in sunlight energy [18]. Numerous reports [19–22] focused on the modification of semiconductor titanium dioxide to enhance its photocatalytic activity have been published.

Since Asahi et al. [23] found that nitrogen doped TiO_2 was conductive to increase the absorption of visible light and photocatalytic activity. Many researches involved in nonmetal doping modification in TiO_2, which are mainly to extend the working spectrum of titanium dioxide in the visible light region, have been done in recent years [24–26]. Especially, nitrogen doped TiO_2 is full of great interest, our previous work has demonstrated that there are two major kinds of nitrogen species doped in TiO_2 [18]. One is the nitrogen doped into TiO_2 lattice to substitute the oxygen (N1), and the other is the nitrogen species chemically adsorbed on the surface of catalyst (N2). The former nitrogen is beneficial, conversely, the latter nitrogen is harmful to the photocatalytic activity of TiO_2 under the visible light irradiation. However, it is very difficult to increase the doping concentration of N1 while decreasing the concentration of N2 in TiO_2, owing to the departing of lattice N1 at a high calcination temperature [27]. With the increase of calcination temperature, the N1 decreases while the N2 increases. Thus, it is against to the enhancing of visible light activity of N–TiO_2. Therefore, it is very difficult to obtain a high ratio of N1/N2 by using traditional methods.

Moreover, Ti^{3+}-self doped TiO_2 has demonstrated the increase in absorption in visible light and attracts a great interest in recent years. Sasikala et al. [28] successfully achieved the evidence of supporting that Ti^{3+} and oxygen vacancies facilitated absorption of visible light for TiO_2–SnO_2. After that, Zuo et al. [29] successfully prepared Ti^{3+} self-doped TiO_2 with high stability, strong absorption of visible light and excellent performance in hydrogen production from photocatalysis water splitting through a one-step method. Xing et al. [30] also obtained modified Ti^{3+} self-doped TiO_2 by a low-temperature vacuum activation method instead of conventional method, which needs high temperature or uneconomical equipment. The catalysts showed high stability of Ti^{3+} and oxygen vacancies and outstanding photoactivity. Moreover, a simple

* Corresponding authors. Tel.: +86 21 64252062; fax: +86 21 64252062.
E-mail addresses: mingyangxing@ecust.edu.cn (M. Xing), jlzhjang@ecust.edu.cn (J. Zhang).

http://dx.doi.org/10.1016/j.apcatb.2015.01.036
0926-3373/

one-step solvent-thermal method using low-cost $NaBH_4$ as a reductant was also reported that can successfully synthesize a series of Ti^{3+} self-doped TiO_2 catalysts. The catalysts also exhibited strong visible light absorption and enhanced photocatalytic activity [31].

Metal and nonmetal co-doping have obtained great progress in the modification of titanium dioxide material [32,33]. Some investigations on the modification of metal and nitrogen co-doped TiO_2 have been reported. Hoang et al. [34] proposed a reversible electron transfer between the paramagnetic bulk species of N (N_b) and Ti^{3+} centers forming the diamagnetic bulk species of N_b^- and Ti^{4+}, and the synergistic effect involving Ti^{3+} and N in TiO_2 nanowire arrays is responsible for the outstanding performance of water photooxidation under visible illumination. Although a great progress regarding the synthesis of Ti^{3+}/nitrogen co-doped TiO_2 has been achieved, the mechanism of co-doped is still controversial.

Herein, it was aimed in the mechanism of nitrogen and Ti^{3+} co-doped TiO_2 to enhance the visible light photocatalytic activity, especially the relationship between the formation of oxygen vacancies and the substitution of nitrogen into TiO_2. A series of Ti^{3+} and nitrogen co-doped TiO_2 catalysts have been obtained by using low-cost ammonium hydroxide as the nitrogen source via a calcination–vacuum activation method. The visible-light photodegradation of methyl orange of the co-doped TiO_2 was enhanced accounted for the synergistic effects between Ti^{3+} and N.

2. Experimental

2.1. Preparation of N, Ti^{3+} co-doped TiO_2

Titanium sulfate (24 g, $Ti(SO_4)_2$) was added to the ultrapure water (120 mL) and the solution was stirred at room temperature for 1 h, and then ammonium hydroxide was added dropwise to the above solution. The suspension with a pH value of 7.0 was obtained by controlling the amount of ammonium hydroxide. After that, the collected solid particles were washed with large amounts of water by vacuum filtration. The precipitates were dried under vacuum at 60 °C for 12 h. The as-dried sample was calcined at 400 °C for 2 h (ramping time 95 min). The obtained nanoparticles of TiO_2 doped with nitrogen are denoted as N–TiO_2.

The final powder was activated in a vacuum tube furnace at 200 °C, 300 °C, 400 °C, 500 °C and 600 °C for 3 h, respectively (ramping time 95 min). Then a series of nitrogen and Ti^{3+}co-doped TiO_2 were obtained and denoted as N–TiO_{2-x} (m-3 h) (m = 100, 200, 300, 400, 500, 600 °C represent the vacuumed temperature). N–TiO_2 powder was calcined in the air at 300 °C for 3 h (ramping time 95 min). And the obtained nanoparticles are denoted as air-N–TiO_2.

2.2. Preparation of Ti^{3+} self-doped TiO_2

Using the same experimental method, in order to control the pH value of 7.0, ammonium hydroxide was replaced by sodium hydroxide. The nano-particles of TiO_2 are denoted as TiO_2. After vacuum activation treatment at 300 °C for 3 h, the Ti^{3+} self-doped TiO_2 was successfully prepared and denoted as TiO_{2-x} (300 °C-3 h).

2.3. Characterization

All prepared samples were measured by a Rigaku D/max 2550 VB/PC diffractometer (Cu K radiation, λ = 1.5406 Å) in the range of 10–80° (2θ) for X-ray diffraction (XRD) patterns. The dry-pressed disk samples were used to test the UV–vis absorbance spectra of the catalysts using $BaSO_4$, as the reflectance sample via a Scan UV–vis spectrophotometer (Shimadzu, UV-2450) equipped with an integrating sphere assemble. And the spectra of the catalysts were recorded at room temperature in air within the range 200–800 nm. A Perkin–Elmer PHI 5000C ESCA system with Al Kα radiation operated at 250 W was used to study the surface constitution of the samples. The shift of the binding energy due to relative surface charging was corrected using the N1s level at 401 eV as an internal standard. The ESR spectra were recorded at room temperature (Varian E-112). The morphologies of catalysts were obtained by transmission electron microscopy (TEM, JEM-1400). Brunauer–Emmett–Teller (BET) surface area measurements were carried out by a Micromeritics ASAP2020 instrument. The pore size distribution was collected by the Barrett–Joyner–Halenda (BJH) method.

2.4. Photocatalytic activity tests

Methyl orange (MO, 10 mg/L) was degraded as simulative pollutant to evaluate the photocatalytic activity of each sample. The photocatalyst sample (0.07 g) was added into a 100 mL quartz photocatalytic reactor with addition of 70 ml MO solution. The mixture was stirred for 30 min in the absence of light in order to achieve the adsorption–desorption equilibrium. The visible light source was provided by a 500-W tungsten halogen lamp with UV cutoff filters (λ > 420 nm). And a 300-W high- pressure Hg lamp, whose strongest emission wavelength was 365 nm, as the UV light source. The photocatalytic system was cooled using flowing water in a quartz cylindrical jacket, and ambient temperature was approximately constant during the photocatalytic reactions. At given intervals, analytical samples were taken from the mixture and immediately centrifuged. The supernatant liquid was analyzed by recording variations in the absorption of the UV–vis spectra for MO by using a Cary 100 UV–vis spectrometer.

3. Results and discussion

3.1. Phase structure

The XRD spectra of various samples are shown in Fig. 1. For each sample, all peaks can be ascribed to the anatase phase of TiO_2. Compared with pure TiO_2, the increase of intensity peak of the N-doped TiO_2 indicates higher crystallinity (Fig. 1a). The vacuum activation cannot change the crystalline structure of TiO_2, even at high temperatures (Fig. 1b). Moreover, the maximum peak intensity of N–TiO_{2-x} (600 °C-3 h) implies the highest crystallinity. The average crystallite sizes are calculated according to the Debye–Scherer equation, as shown in Table 1.

The result obtained is in line with the report that the nonmetal doping modifications could cause a decrease in particle size [35]. That is, the N-doped TiO_2 shows a smaller particle size than pure TiO_2. The lattice deformation and oxygen vacancies in the anatase crystallites can lead to the decrease of particle size [36]. The doping of nitrogen may restrain the growth of crystals. Conversely, the particle size of vacuum activated TiO_2 is almost changeless in comparison with the value of pure TiO_2. In addition, with the increase of the temperature about vacuum activation, the particle sizes of

Table 1
Measured structural characteristics of the various samples.

Samples	Particle size (nm)	(1 0 1) d-spacing (Å)
TiO_2	24.1	3.5
N–TiO_2	19.6	3.5
TiO_{2-x} (300 °C-3 h)	25.0	3.5
N–TiO_{2-x} (100 °C-3 h)	20.6	3.5
N–TiO_{2-x} (200 °C-3 h)	19.4	3.5
N–TiO_{2-x} (300 °C-3 h)	19.8	3.5
N–TiO_{2-x} (400 °C-3 h)	20.1	3.5
N–TiO_{2-x} (500 °C-3 h)	21.8	3.5
N–TiO_{2-x} (600 °C-3 h)	30.4	3.5

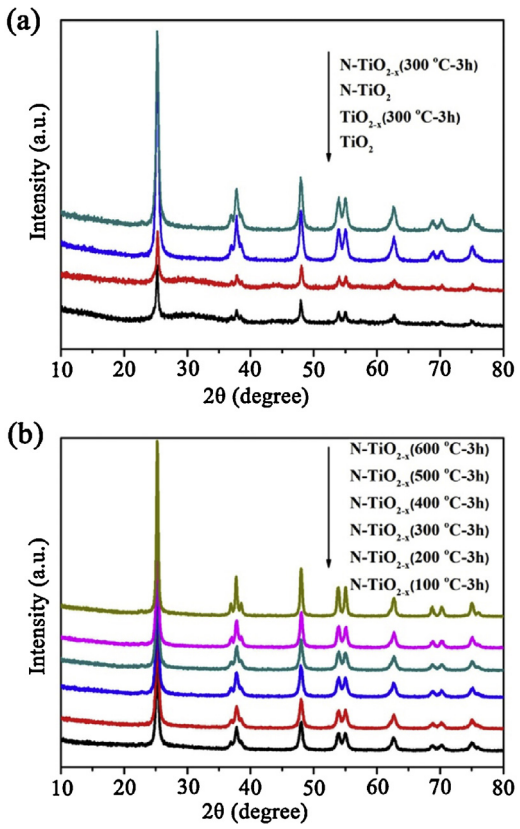

Fig. 1. XRD patterns of (a) TiO_2, N-doped TiO_2, TiO_{2-x}, N–TiO_{2-x} (b) N-doped TiO_2 vacuum activated at different temperatures.

N–TiO_{2-x} decrease at first, but then are inclined to increase. When the temperature is higher than 400 °C, there is a significant increase of particle size and the N–TiO_{2-x} (600 °C-3 h) represents the largest size, which means that the high temperature is beneficial to either the crystallization or the growth of the crystal. During the vacuum activation, the generation of Ti^{3+} and oxygen vacancy is beneficial to the substitution of nitrogen into TiO_2, which can further decrease the particle size of co-doped catalysts. Furthermore, the value of the "*d*" space is almost changeless, which elaborates that the doping of either nitrogen or Ti^{3+} cannot change the average unit cell dimension [22]. The N–TiO_{2-x} (300 °C-3 h) can be recorded by TEM images, shown in Fig. 2. The N–TiO_{2-x} samples exhibit a uniform size at the level of the XRD observation and the particle size of the catalyst is about 19.8 nm.

The N_2 adsorption–desorption isotherms and BJH pore size distribution (PSD) curves of these samples are employed to investigate the pore structure of N–TiO_{2-x} vacuum activated at different temperatures (Fig. 3). As a result, all of the isotherms are of the Type II according to the IUPAC classification. And the absorption of N_2 in the analysis can be ascribed to the inter-aggregated pores which are structured by the neighboring nanoparticles. Additionally, the surface area and the BJH pore size of the N–TiO_{2-x} vacuum activated at different temperatures are all similar with each other. It can be considered that the substitution of nitrogen for oxygen vacancies into the TiO_2 leads to a higher visible-light photocatalytic activity instead of differences of pore structure.

3.2. Optical property

The UV–vis diffuse reflectance spectra of different samples are presented in Fig. 4. The comparison between N-doped TiO_2 and pure TiO_2 shows that absorption intensity in the range of

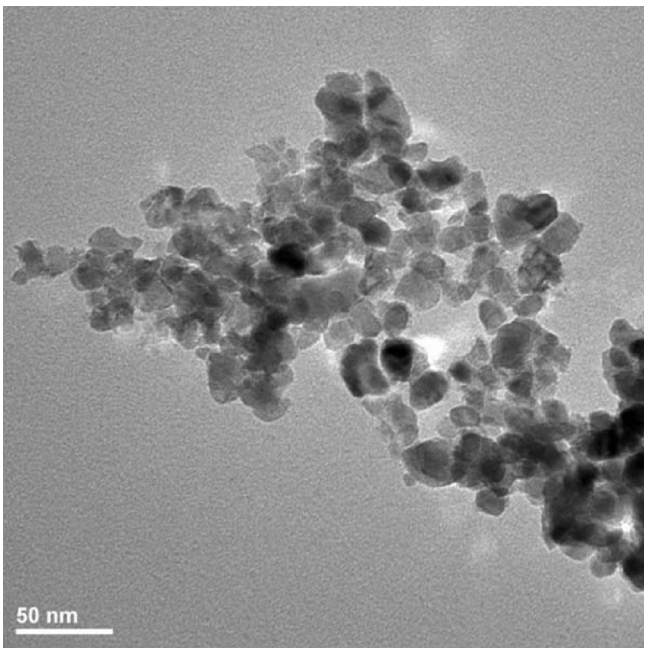

Fig. 2. TEM images of the N–TiO_{2-x} (300 °C-3 h).

400–550 nm of TiO_2 obviously increases with nitrogen doping. And the N-doped TiO_2 also shifts the absorption edge further to the longer wavelength region (~550 nm). It may be attributed to the generation of some nitrogen species or color spots on the surface of the catalyst. Additionally, compared with pure TiO_2, the absorption intensity of the vacuum activated TiO_2 (TiO_{2-x}) also obviously increases in the wide range of 400–750 nm, which results from the generation of Ti^{3+} and oxygen vacancies. The result is consistent with the reports of Zuo et al. [29] and our previous works [30]. Zuo et al. adopted a one-step method to synthesize Ti^{3+} self-doped TiO_2. In addition to that, Xing et al. used a vacuum activation method for modifying P25 to obtain Ti^{3+} self-doped TiO_2. Furthermore, with the increase of activation temperature, the absorption intensity in the visible region enhances at first, but recedes later. The N–TiO_{2-x} (300 °C-3 h) and the N–TiO_{2-x} (600 °C-3 h) are the strongest and the weakest, respectively. The synergistic effect involving Ti^{3+} and nitrogen in TiO_2 results in the significant enhancement of absorption intensity in the visible-light region of catalyst. The result implies that the catalyst calcinated at 300 °C possesses the maximum amount of Ti^{3+}. When vacuum activation temperature is higher than 300 °C, the amount of Ti^{3+} doping decreases.

3.3. Chemical composition

ESR is employed to investigate the generation of the Ti^{3+} and oxygen vacancy on the vacuum activated samples (Fig. 5). No signal is shown for the pure TiO_2 catalyst at $g = 1.992$, while vacuum activated sample (TiO_{2-x} (300 °C-3 h)) exhibits a stronger signal as the same as the intensity of the feature at a *g*-value of 1.992 for paramagnetic Ti^{3+} center has been widely reported [34,37,38]. It implies that the generation of Ti^{3+} is attributed to vacuum activation. It proves that the increase of absorption intensity of the catalyst in visible light region is the result of Ti^{3+} self-doping. Compared with TiO_{2-x} (300 °C-3 h), N–TiO_{2-x} gives rise to a stronger ESR signal, which indicates that vacuum activation is beneficial for the substitution of nitrogen for oxygen vacancy in TiO_2 as well as the generation of Ti^{3+} for the reason of charge balance. It is worth noting that the strongest ESR signal possessed by sample activated at 300 °C among different activation temperature. It can be claimed that N–TiO_{2-x} (300 °C-3 h) contains the highest Ti^{3+} concentration.

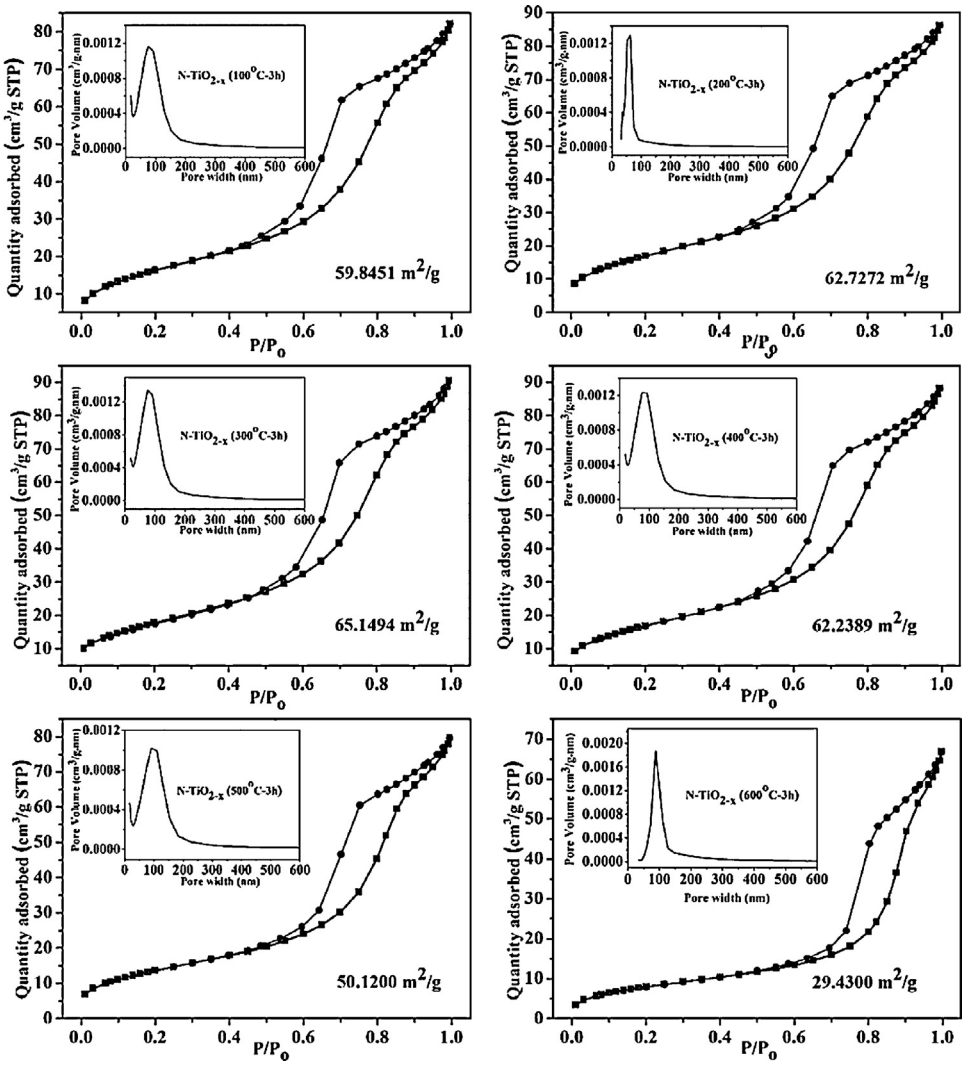

Fig. 3. N_2 adsorption–desorption isotherms of N–TiO_2 catalysts vacuum activated at different temperatures. Insert spectra are the BJH pore size distribution curves of corresponding samples.

In another word, the highest concentration of Ti^{3+} corresponds to the strongest absorption intensity of catalyst in visible-light region.

XPS characterization is used to investigate the composition of N/Ti^{3+} co-doped TiO_2 catalyst. The peak from N1s is detected in the survey scan from the surface and subsurface of N–TiO_2, air-N–TiO_2 and N–TiO_{2-x}, as shown in Fig. 6. There is a broad peak from 396.5 eV to 404.5 eV in N–TiO_2, which is considered to be the typical peak of N-doped TiO_2 reported by several papers [23,39,40]. After fitting of the curve, two intense peaks at 398.7 eV and 400.5 eV are observed for N–TiO_2 and N–TiO_{2-x} which is consistent with the N1s binding energy region. It implies that there are two states of nitrogen doping in the TiO_2. One is nitrogen doping into lattice of TiO_2 (N1) and the other is chemically adsorbed on the surface of the catalyst (N2), which can be observed at 398.7 eV and 400.5 eV, respectively. Herein, the intense peak at 398.7 eV by reason of anionic N-in O–Ti–N has been reported by other researcher [41]. Moreover, the peak at 400.5 eV is attributed to the oxidized nitrogen of Ti–O–N in our previous study [18]. It has been reported that the two states of nitrogen doped in TiO_2 are all regarded as the important factors to affect the photocatalytic activity of TiO_2 under the visible light illumination [27]. Interestingly, a comparison of the curve between N–TiO_2 and N–TiO_{2-x} shows a stronger peak at 398.7 eV and a weaker peak at 400.5 eV can be observed after vacuum activation (Fig. 6a). However, the total N atom percentage is almost changeless after being activated in the vacuum for 3 h (N/Ti ratio changes from 0.022 to 0.023). The results demonstrate that the vacuum activation facilitates the further doping of nitrogen into the lattice of TiO_2. It can be speculated that the increase of the Ti–N (Fig. 6a) is attributed to the substitution of nitrogen for oxygen vacancies into the TiO_2 lattice during the vacuum activation process. In addition, the total nitrogen atom percentage of N–TiO_2 and air-N–TiO_2 is 0.86% and 0.42%, respectively. Compared with the N–TiO_2, the air-N–TiO_2 shows an obvious lower total nitrogen atom percentage. It indicates that the nitrogen in the air cannot be doping into the lattice of TiO_2 by calcination even if nitrogen exists in the air around the surface of samples, which is also be confirmed by several reports [42,43]. In addition, compared with the N–TiO_{2-x}, air-N–TiO_2 shows a weaker peak at 398.7 eV and a stronger peak at 400.5 eV (Fig. 6b), which demonstrates that the nitrogen atom chemically absorbed on the surface of the catalyst can further replace the oxygen vacancy sites at a high heating temperature in the vacuum condition. Compared with the pure TiO_2, the total O atom percentage of N–TiO_2 obviously decreases after nitrogen doping (O/Ti ratio changes from 3.20 to 2.91). It can be inferred that the nitrogen replaces the oxygen atoms into the surface or subsurface lattice of TiO_2 during the calcination treat-

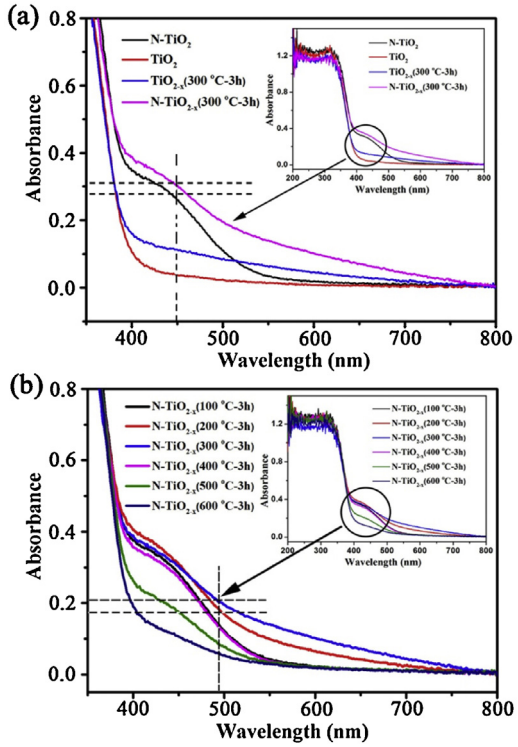

Fig. 4. UV–vis diffuse reflectance spectra and the amplification in the visible-light region of various samples (a) TiO_2, N–TiO_2, TiO_{2-x}, N–TiO_{2-x} (b) N-doped TiO_2 vacuum activated at different temperatures.

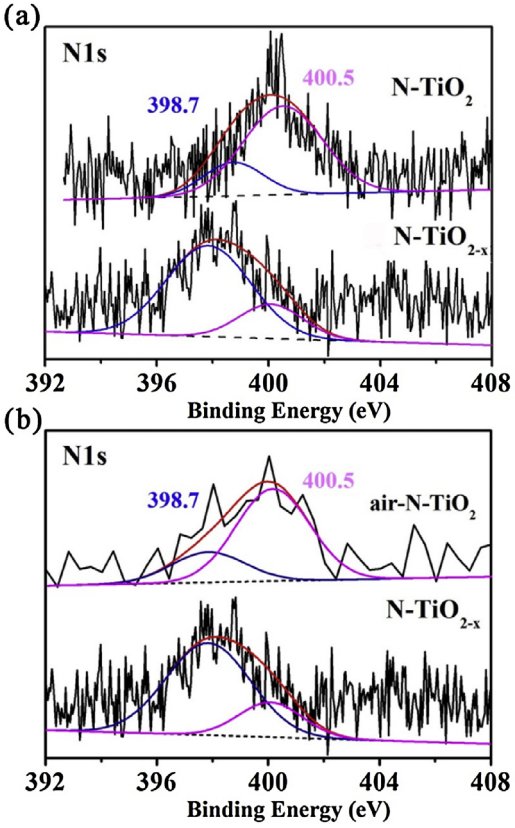

Fig. 6. N1s XPS spectra of N–TiO_2, N–TiO_{2-x} and air-N–TiO_2.

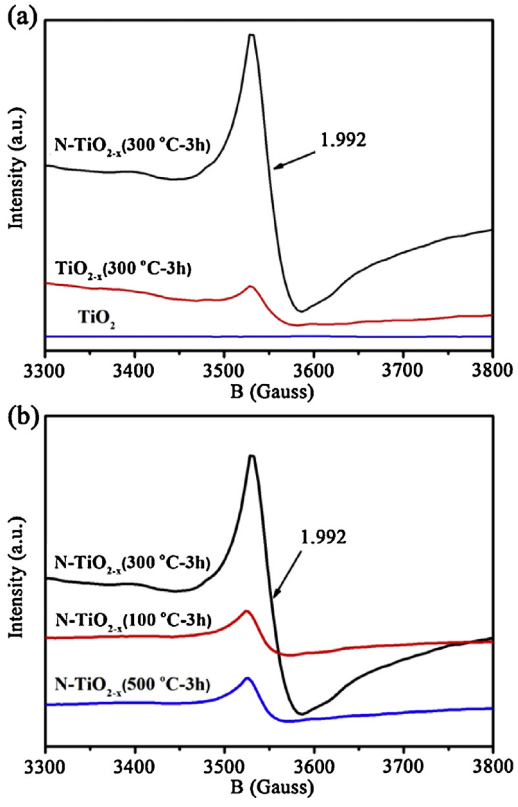

Fig. 5. ESR spectra of (a) TiO_2, TiO_{2-x} (300 °C-3 h), N–TiO_{2-x} (300 °C-3 h) and (b) different samples vacuum activated at different temperature.

ment in air, which leads to a decrease of O atom percentage in N–TiO_2. To the N–TiO_2, some nitrogen atoms squeeze into the lattice interval of TiO_2, firstly in the beginning of the air calcination, as shown in Fig. 7. With the increase of calcination temperature in air, the neighbor oxygen atoms are departing from the lattice and the interval nitrogen is substitutions for the sites of oxygen atoms. As a result, the nitrogen successfully achieves the substitution of nitrogen for oxygen atoms (N1). Meanwhile, some other nitrogen atoms are chemically adsorbed on the surface of TiO_2 (N2), as the peak of 400.5 eV shown in the Fig. 6a. After that, the N–TiO_2 is put into the vacuum tube furnace to be activated at different temperatures. During the vacuum activation process, some oxygen atoms are departed from the lattice of TiO_2 to form some oxygen vacancies due to the negative pressure at a heating temperature (Fig. 7). Moreover, the percentage of nitrogen doping into lattice of TiO_2 (N1) and chemically adsorbed on the surface of the catalyst (N2) was obtained by the calculation [18]. As a result, the percentages of N1 in N–TiO_2 and N–TiO_{2-x} are 0.56 at% and 0.18 at%, respectively. And the amount of N2 in N–TiO_2 and N–TiO_{2-x} are 0.17 at% and 0.67 at%, respectively. Because of the formation of oxygen vacancies, the percentage of nitrogen species adsorbed on the surface of TiO_2 (N2) is substitutions of these oxygen vacancies to enhance the percentage of the nitrogen doped into the lattice of TiO_2 (N1) after the vacuum activation, with the total nitrogen atom percentage almost changeless. It leads to the increase of peak at 398.7 eV after vacuum activation in Fig. 6a. In other aspect, the extra electron in nitrogen will transfer to the neighbor Ti^{4+} to generate Ti^{3+} to achieve the charge balance, which is consistent with the ESR results that the N–TiO_{2-x} has a strong Ti^{3+} signal in Fig. 5a. Hence, the vacuum activation method is a useful technology to enhance the substitution of nitrogen into TiO_2, which is expected to be beneficial to the visible-light photocatalytic activity of TiO_2.

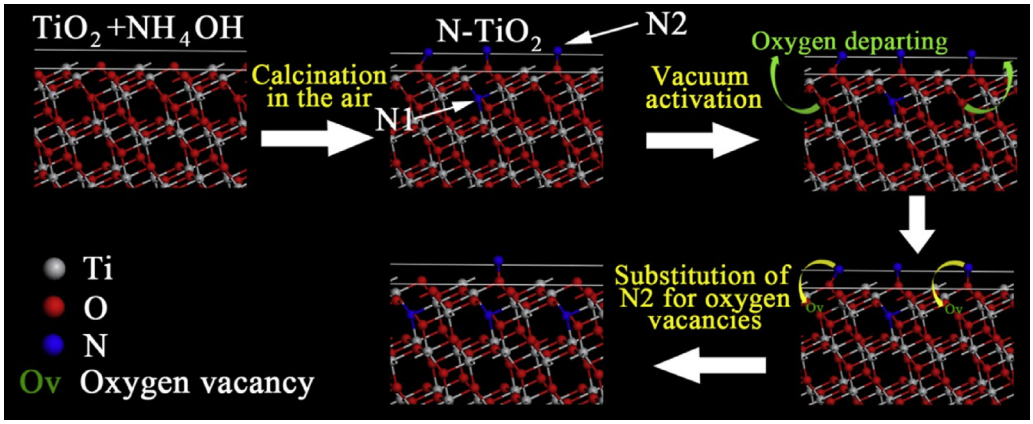

Fig. 7. Proposed anatase crystal (1 0 1) surface structural model of TiO_2, N–TiO_2 and N–TiO_{2-x}, and a schematic diagram of the substitution of nitrogen for oxygen vacancies during the vacuum activation.

3.4. Photocatalytic activity of N–TiO_{2-x}

The photocatalytic activity of the Ti^{3+} and nitrogen co-doped samples is evaluated by the degradation of organic pollutants (MO) under visible light irradiation ($\lambda > 425$ nm). Fig. 8a shows the relative changes of MO concentrations with irradiation time. And all the catalysts show a very low and similar adsorption for methyl orange (MO) in the dark (Fig. 9). Compared with the pure TiO_2, either N–TiO_2 or N–TiO_{2-x} shows a higher photo degradation rate for MO under visible light illumination. After a simple vacuum activation, the TiO_{2-x} gives a higher photocatalytic activity owing to the generation of Ti^{3+}. To the N–TiO_2, it can be considered that the nitrogen replaces the oxygen atoms in TiO_2. As a result, the band gap of TiO_2 is reduced after nitrogen doping, leading to an efficient visible light photocatalytic activity [23,30]. Furthermore, the catalysts show the higher photocatalytic activity after vacuum activation, resulting from the synergistic effect between Ti^{3+} and nitrogen into TiO_2 lattice. As can be seen in XPS spectra (Fig. 6a), there is an obvious increase of the nitrogen of N1 and a decrease of the nitrogen of N2 after vacuum activation. That is, the ratio of N1/N2 significantly increases after vacuum activation, which is beneficial to the enhancing of visible-light activity of TiO_2 [18]. The enhancing nitrogen doping into TiO_2 lattice after vacuum activation shows an increase of absorption in visible light region, and an enhancing visible light photocatalytic activity (Fig. 8b) shows the degradation of MO for the nitrogen doped TiO_2 after vacuum activation at different temperatures under visible light illumination. It can be seen that with the increase of vacuum activation temperature, photocatalytic activity firstly increases and then decreases. Under the optimized treating condition, the catalyst N–TiO_{2-x} (300 °C-3 h) exhibits the highest photocatalytic activity. On the contrary, the sample N–TiO_{2-x} (600 °C-3 h) shows almost no activity owing to the bigger particle size and lower Ti^{3+} concentration. When vacuum activation temperature increases, the particle sizes increase and the generation of Ti^{3+} decreases (Fig. 5b). As a result, the corresponding photocatalytic activity is reduced [27,44]. Because of the large particle size, the recombination rate of the photo-produced carriers in the bulk of TiO_2 increases significantly, which results in the decrease of photocatalytic activity.

Fig. 10 shows the changes of the relative concentrations of MO under the UV light irradiation. Compared with pure TiO_2, nitrogen doped TiO_2 exhibits higher activity under UV light illumination. That is because the introduction of nitrogen doping level into the bandgap of TiO_2 facilitates the separation of electrons and holes.

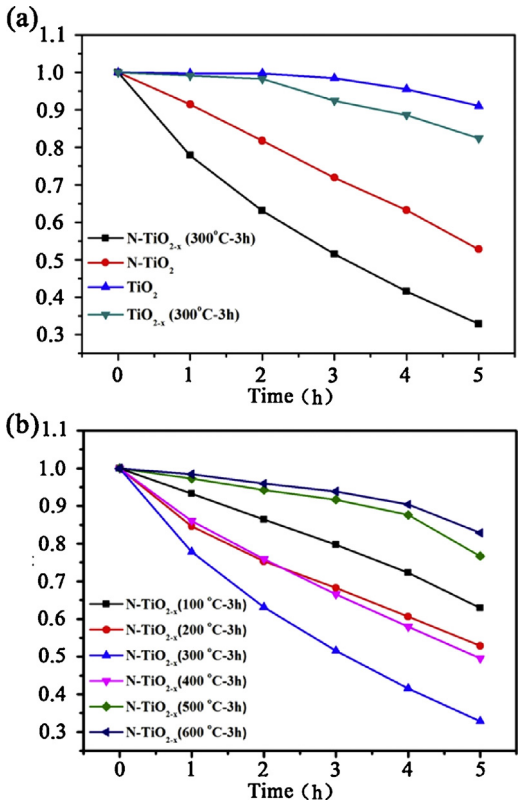

Fig. 8. (a) Visible light photocatalytic activities of TiO_2, N–TiO_2, N–TiO_{2-x} and (b) N–TiO_2 catalysts vacuum activated at different temperatures.

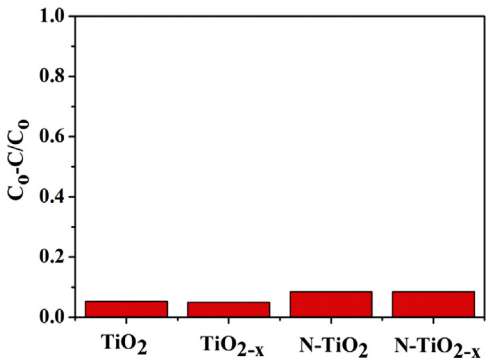

Fig. 9. The adsorption capacity for methyl orange (MO) on different samples in the dark.

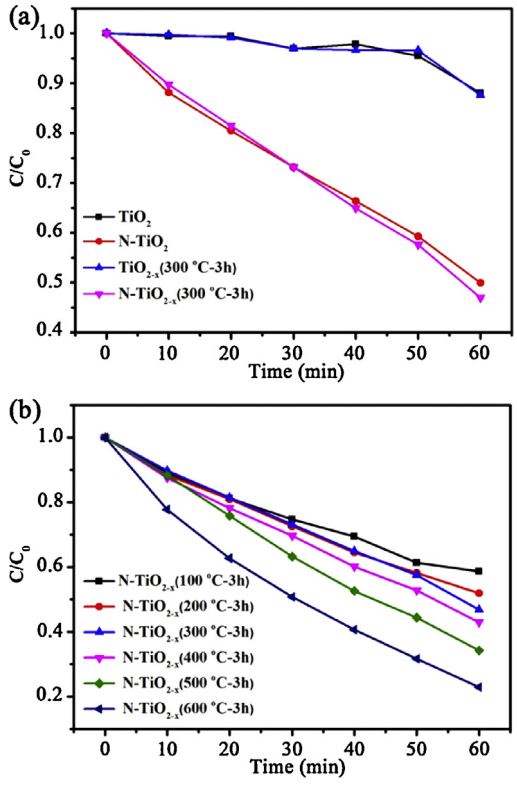

Fig. 10. (a) Ultraviolet light photocatalytic activities of TiO_2, N–TiO_2, N–TiO_{2-x} and (b) N–TiO_2 catalysts vacuum activated at different temperatures.

At the same time, the UV-light photoactivity of the samples after vacuum activation is almost changeless. Ti^{3+} self-doping and the further doping of nitrogen cannot introduce carrier recombination centers, therefore, it is different from other metal doping [45,46]. Fig. 10b shows the changes of the relative concentrations of MO with irradiation time for N–TiO_2 after vacuum activation at different temperatures. The result exhibits that photocatalytic activity of the samples increases smoothly. With the increase of vacuum activation temperature, there is a phenomenon that the photocatalytic activity of the catalysts increases under ultraviolet illumination, which is similar to the trend of catalytic crystalline, and it reaches the maximum at 600 °C (Fig. 1b). It indicates that high crystalline contributes to high photoactivity in that the decrease of lattice defects in the bulk of TiO_2, which is beneficial to the separation of electrons and holes under the circumstance that there is a large number of carries produced under the UV light irradiation.

The donor level induced by nitrogen doping upon the VB exists inside the bandgap of TiO_2, where electrons are generated under the irradiation of visible light (Fig. 11). Meanwhile, Ti^{3+} self-doping introduces an impurity level under the CB which can trap the photo-induced electrons. At the same time, it can reduce oxygen and produce a superoxide radical which promotes the separation of charge carrier, while holes left in the VB accelerate the generation of free OH radicals. The band gap is narrowed by the existence of N doping level and the Ti^{3+} impurity level, which can enhance photocatalytic activity of TiO_2. The N doping can improve the absorption of visible light, and the Ti^{3+} doping can enhance the separation efficiency of photo-generate electrons and holes. It is well worth mentioned that the nitrogen could be further doped into TiO_2 lattice by the substitution of oxygen vacancies during the vacuum activation process, which can further improve the concentration of doping levels inside the bandgap of TiO_2. Hence, the synergistic effect between Ti^{3+} and nitrogen is responsible for the high visible light and UV light photocatalytic activity of TiO_2.

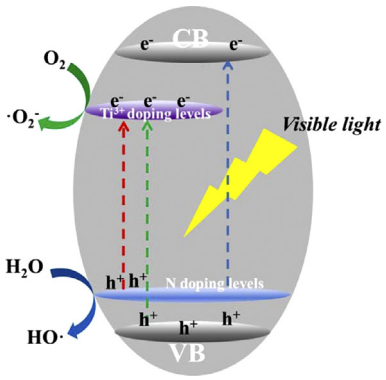

Fig. 11. Proposed structural model of energy states that exist between the VB and CB of N–TiO_{2-x}, and a schematic diagram of the charge separation and photocatalytic activity of the photocatalyst.

4. Conclusions

In summary, the N–TiO_{2-x} is successfully prepared by using the calcination–vacuum activation method. The vacuum activation technology is confirmed that it can improve the substitution of nitrogen for oxygen vacancies into the TiO_2 and decrease the chemically adsorbed nitrogen species, which leads to a higher visible-light photocatalytic activity than the pure TiO_2 and the N–TiO_2. A Ti^{3+} impurity level is introduced by the vacuum activation treatment. And plenty of nitrogen is doped into the lattice of TiO_2. The N–TiO_{2-x} catalysts have high photocatalytic activities for the degradation of methyl orange under the visible-light and the UV-light irradiation. The synergistic effect between Ti^{3+} and nitrogen doping is responsible for the high visible light activity of N–TiO_{2-x} (300 °C-3 h), and the high crystallinity is the reason for the high UV light activity of N–TiO_{2-x} (600 °C-3 h).

Acknowledgements

This work has been supported by National Nature Science Foundation of China (21237003, 21203062, 21377038, 21173077), the Research Fund for the Doctoral Program of Higher Education(20120074130001) and the Fundamental Research Funds for the Central Universities.

References

[1] A. Fujishima, K. Honda, Nature 238 (1972) 37–38.
[2] J. Schneider, M. Matsuoka, M. Takeuchi, J.-L. Zhang, Y. Horiuchi, M. Anpo, D.W. Bahnemann, Chem. Rev. 114 (2014) 9919–9986.
[3] A. Kudo, Y. Miseki, Chem. Soc. Rev. 38 (2009) 253–278.
[4] R. Daghrir, P. Drogui, D. Robert, Chem. Res. 52 (2013) 3581–3599.
[5] A. Selvaraj, S. Sivakumar, A.K. Ramasamy, V. Balasubramanian, Res. Chem. Intermed. 39 (2013) 2287–2302.
[6] J. Senthilnathan, L. Philip, Chem. Eng. J. 172 (2011) 678–688.
[7] D. Dolat, S. Mozia, B. Ohtani, A.W. Morawski, Chem. Eng. J. 225 (2013) 358–364.
[8] T. Maggos, A. Plassais, J.G. Bartzis, C. Vasilakos, N. Moussiopoulos, L. Bonafous, Environ. Monit. Assess. 136 (2008) 35–44.
[9] N. Todorova, T. Vaimakis, D. Petrakis, S. Hishita, N. Boukos, T. Giannakopoulou, M. Giannouri, S. Antiohos, D. Papageorgiou, E. Chaniotakis, C. Trapalis, Catal. Today 209 (2013) 41–46.
[10] J.V.S. de Melo, G. Trichês, Build. Environ. 49 (2012) 117–123.
[11] N. Li, G. Liu, C. Zhen, F. Li, L. Zhang, H.-M. Cheng, Adv. Funct. Mater. 21 (2011) 1717–1722.
[12] N.G. Park, J. van de Lagemaat, A.J. Frank, J. Phys. Chem. B 104 (2000) 8989–8994.
[13] J.T.-W. Wang, J.M. Ball, E.M. Barea, A. Abate, J.A. Alexander-Webber, J. Huang, M. Saliba, I. Mora-Sero, J. Bisquert, H.J. Snaith, R.J. Nicholas, Nano Lett. 14 (2013) 724–730.
[14] S.L. Fischer, C.P. Koshland, Environ. Sci. Technol. 41 (2007) 3121–3126.
[15] J. Huo, Y. Hu, H. Jiang, X. Hou, C. Li, Chem. Eng. J. 258 (2014) 163–170.
[16] J. Wang, D.N. Tafen, J.P. Lewis, Z. Hong, A. Manivannan, M. Zhi, M. Li, N. Wu, J. Am. Chem. Soc. 131 (2009) 12290–12297.

[17] J. Lin, R. Zong, M. Zhou, Y. Zhu, Appl. Catal. B 89 (2009) 425–431.
[18] M. Xing, J. Zhang, F. Chen, Appl. Catal. B 89 (2009) 563–569.
[19] A. Fujishima, X. Zhang, D.A. Tryk, Surf. Sci. Rep. 63 (2008) 515–582.
[20] M.A. Henderson, J.M. White, H. Uetsuka, H. Onishi, J. Am. Chem. Soc. 125 (2003) 14974–14975.
[21] S. Sakthivel, H. Kisch, Angew. Chem. Int. Ed. 42 (2003) 4908–4911.
[22] M. Sathish, B. Viswanathan, R.P. Viswanath, C.S. Gopinath, Chem. Mater. 17 (2005) 6349–6353.
[23] R. Asahi, T. Morikawa, T. Ohwaki, K. Aoki, Y. Taga, Science 293 (2001) 269–271.
[24] K. Nagaveni, M.S. Hegde, N. Ravishankar, G.N. Subbanna, G. Madras, Langmuir 20 (2004) 2900–2907.
[25] A. Fattori, L.M. Peter, H. Wang, H. Miura, F. Marken, J. Phys. Chem. C 114 (2010) 11822–11828.
[26] H. Irie, Y. Watanabe, K. Hashimoto, J. Phys. Chem. B 107 (2003) 5483–5486.
[27] S.-K. Joung, T. Amemiya, M. Murabayashi, K. Itoh, Appl. Catal. A 312 (2006) 20–26.
[28] R. Sasikala, A. Shirole, V. Sudarsan, T. Sakuntala, C. Sudakar, R. Naik, S.R. Bharadwaj, Int. J. Hydrogen Energy 34 (2009) 3621–3630.
[29] F. Zuo, L. Wang, T. Wu, Z. Zhang, D. Borchardt, P. Feng, J. Am. Chem. Soc. 132 (2010) 11856–11857.
[30] M. Xing, J. Zhang, F. Chen, B. Tian, Chem. Commun. 47 (2011) 4947–4949.
[31] M. Xing, W. Fang, M. Nasir, Y. Ma, J. Zhang, M. Anpo, J. Catal. 297 (2013) 236–243.
[32] P. Zhang, S. Yin, T. Sekino, S. Lee, T. Sato, Res. Chem. Intermed. 39 (2013) 1509–1515.
[33] P. Songkhum, J. Tantirungrotechai, Res. Chem. Intermed. 39 (2013) 1555–1561.
[34] S. Hoang, S.P. Berglund, N.T. Hahn, A.J. Bard, C.B. Mullins, J. Am. Chem. Soc. 134 (2012) 3659–3662.
[35] M. Fernandez-Garcia, A. Martinez-Arias, J. Hanson, J. Rodriguez, Chem. Rev. 104 (2004) 4063–4104.
[36] M.Y. Xing, W.K. Li, Y.M. Wu, J.L. Zhang, X.Q. Gong, J. Phys. Chem. C 115 (2011) 7858–7865.
[37] J. Conesa, J. Soria, J. Phys. Chem. 86 (1982) 1392–1395.
[38] I. Nakamura, N. Negishi, S. Kutsuna, T. Ihara, S. Sugihara, K. Takeuchi, J. Mol. Catal. A: Chem. 161 (2000) 205–212.
[39] Y. Cong, L. Xiao, J. Zhang, F. Chen, M. Anpo, Res. Chem. Intermed. 32 (2006) 717–724.
[40] K. Aoki, T. Morikawa, T. Ohwaki, Y. Taga, Chem. Lett. 35 (2006) 616–617.
[41] C. Burda, Y. Lou, X. Chen, A.C.S. Samia, J. Stout, J.L. Gole, Nano Lett. 3 (2003) 1049–1051.
[42] Z.B. Wu, F. Dong, W.R. Zhao, H.Q. Wang, Y. Liu, B.H. Guan, Nanotechnology 20 (2009) 235701.
[43] C. Chen, H. Bai, C. Chang, J. Phys. Chem. C 111 (2007) 15228–15235.
[44] Y. Zhao, X. Qiu, C. Burda, Chem. Mater. 20 (2008) 2629–2636.
[45] Y. Ma, J. Zhang, B. Tian, F. Chen, L. Wang, J. Hazard. Mater. 182 (2010) 386–393.
[46] Y. Cong, J. Zhang, F. Chen, M. Anpo, J. Phys. Chem. C 111 (2007) 6976–6982.